Journal of
Synchrotron Radiation

ISSN 0909-0495

Received 25 November 2008
Accepted 5 January 2009

Phosphorus $L_{2,3}$-edge XANES: overview of reference compounds

Jens Kruse,[a]* Peter Leinweber,[a] Kai-Uwe Eckhardt,[a] Frauke Godlinski,[b] Yongfeng Hu[c] and Lucia Zuin[c]

[a]University of Rostock, Institute for Land Use, 18059 Rostock, Germany, [b]Julius Kühn-Institute, Institute for Crop and Soil Science, 38116 Braunschweig, Germany, and [c]Canadian Light Source, University of Saskatchewan, Saskatoon, SK, Canada S7N 0X4. E-mail: jens.kruse@uni-rostock.de

Synchrotron-based X-ray absorption near-edge structure (XANES) spectroscopy is becoming an increasingly used tool for the element speciation in complex samples. For phosphorus (P) almost all XANES measurements have been carried out at the *K*-edge. The small number of distinctive features at the P *K*-edge makes in some cases the identification of different P forms difficult or impossible. As indicated by a few previous studies, the P $L_{2,3}$-edge spectra were richer in spectral features than those of the P *K*-edge. However, experimentally consistent spectra of a wide range of reference compounds have not been published so far. In this study a library of spectral features is presented for a number of mineral P, organic P and P-bearing minerals for fingerprinting identification. Furthermore, the effect of radiation damage is shown for three compounds and measures are proposed to reduce it. The spectra library provided lays a basis for the identification of individual P forms in samples of unknown composition for a variety of scientific areas.

Keywords: P *L*-edge; NEXAFS; radiation damage; soil P.

1. Introduction

Phosphorus (P) compounds are indispensable components in a vast quantity of chemical, life, technical and environmental processes and reactions. Since P is an essential element in the metabolism of living organisms, P applications as fertilizer to increase field crop yields or additives to enhance the performance of livestock contribute to feed an increasing population on earth. Although these P inputs to agroecosystems are beneficial, imbalances can also cause serious environmental problems (Sims *et al.*, 1998; Dougherty *et al.*, 2004; Godlinski *et al.*, 2004; Nordstrom & Hotta, 2004). Therefore, both the urgency of P supply to the agriculture and food industry on the background of limited resources and possible environmental problems from P loading of vulnerable ecosystems have stimulated research on P cycling in the environment. The most common analytical methods for the chemical characterization of P compounds are sequential fractionations (*e.g.* Hedley & Stewart, 1982) and ^{31}P nuclear magnetic resonance (NMR) spectroscopy (*e.g.* Toor *et al.*, 2006). However, the validity of sequential fractionations is limited by the operational definition of P forms, likely unspecific to particular P species (Hunger *et al.*, 2005). Solid-state ^{31}P-NMR is of low sensitivity and the results of solution-state ^{31}P-NMR depend on the sample pre-treatment (Cade-Menun & Preston, 1996; Leinweber *et al.*, 1997).

The X-ray absorption near-edge structure (XANES) spectroscopy [synonymous to near-edge X-ray absorption fine structure (NEXAFS) spectroscopy] may offer a possibility to overcome specific limitations of the above methods to gain insight into the chemical structure and composition of P compounds in all kinds of samples. In general, XANES is a molecular-scale spectroscopy technique that yields electronic and structural information on the element of interest by using tunable synchrotron light (Schulze & Bertsch, 1995). Each XANES spectrum is usually characterized by intense resonance features, arising from excitations of core-level electrons to unoccupied orbital and continuum levels and from multiple scattering of the emitted photoelectrons by the geometrical arrangement of neighbouring atoms around the absorbing atom. The energy position of the resonance features is related to the chemical environment of the absorber (Stöhr, 1992; Fendorf & Sparks, 1996). This specificity as well as the minimal sample preparation required and the increased accessibility to high-brightness synchrotron beamlines has increased the popularity of XANES spectroscopy to differentiate various elements and their compounds. P XANES offers great possibilities for many science areas because P is relevant not only in

bio- and environmental sciences but also in material science, chemical weapons and medicine.

Most synchrotron-based P XANES studies have been focused on the *K*-edge (~2150 eV) where the P $1s \rightarrow 3p$ transition is probed. The P *K*-edge XANES has been widely utilized to speciate P forms in material science (*e.g.* Najman *et al.*, 2002; Pereira *et al.*, 2007; Lavrentyev *et al.*, 2000), medicine (*e.g.* Siritapetawee & Pattanasiriwisawa, 2008) and environmental science (*e.g.* Beauchemin *et al.*, 2003; Khare *et al.*, 2005; Shober *et al.*, 2006; Kruse & Leinweber, 2008). However, in some cases the speciation of P forms, particularly organic P, was difficult or even impossible at the P *K*-edge XANES because of the lack of distinguishable features in the selected reference compounds (Beauchemin *et al.*, 2003; Ajiboye *et al.*, 2008; Kruse & Leinweber, 2008). XANES at the $L_{2,3}$-edge instead of the *K*-edge seemed to be more promising because the $L_{2,3}$-edge spectra showed more distinguishable features (Fuller *et al.*, 1998; Ajiboye *et al.*, 2006; Kruse *et al.*, 2008; Li *et al.*, 2008). Previously, P *L*-edge XANES was used mainly in material science to specify P compounds in wear films (*e.g.* Kasrai *et al.*, 1999; Varlot *et al.*, 2001; Yin *et al.*, 1997) and glasses (*e.g.* Yin *et al.*, 1993, 1995; Carta *et al.*, 2005). However, to the best of our knowledge there are only a few promising preliminarily results published on the P $L_{2,3}$-edge for environmental samples (Ajibyoe *et al.*, 2006; Schefe *et al.*, 2008). Furthermore, most of the above-cited researchers, who published a few reference spectra along with spectra of unknown composition, emphasized that a high-quality experimentally consistent spectra library of reference compounds is a fundamental pre-requisite for any P speciation in a sample of unknown composition. Such a library of $L_{2,3}$-edge spectra is not yet available.

Furthermore, XANES has often been referred to as a non-destructive method. However, several XANES studies have shown that the energy impact of the X-rays can cause significant changes in the chemistry of the sample (*e.g.* Ascone *et al.*, 2003; Zubavichus *et al.*, 2004). These X-ray-induced chemical changes might generally become more of an issue as the X-ray sources become brighter and more energy will be transferred to the sample. To the best of our knowledge, possible impacts of X-rays during a P XANES experiment have not been systematically studied so far, neither at the *K*- nor at the *L*-edge.

Therefore, the objectives of the present study were (i) to provide a systematic overview of spectral features of a wide range of environmentally and technically relevant P-containing compounds to serve upcoming studies in this and other research areas, and (ii) to investigate if and to what extent the beam impact may alter the spectral features in the P $L_{2,3}$-edge XANES.

2. Experimental

All the reference compounds were purchased from established chemical manufacturers and used without further purification. The CAS (Chemical Abstracts Services) numbers are given in Table 1. The chemical structures are presented next to the spectra in Figs. 1 to 7. All P minerals used in this study were provided by the Institute of Geography and Geology (University of Greifswald, Germany) and originate from well known geological sources. All samples were ground to a very fine powder using an agate stone mortar and spread as a very thin film onto a double-sided P-free carbon tape (G3939, Plano GmbH, D-35578 Wetzlar, Germany) to minimize self-absorption effects. The carbon tape was attached to a 10 mm-diameter stainless steel sample holder which finally was inserted into the X-ray absorption vacuum chamber (base pressure: 2×10^{-8} torr).

The P $L_{2,3}$-edge XANES measurements were performed at the Canadian Light Source (CLS) (Saskatoon, Canada) on the Variable Line Spacing Plane Grating Monochromator (VLS PGM) beamline. This beamline uses a 185 mm planar undulator and three gratings to cover a photon energy range of 5.2 to 250 eV. This beamline is capable of providing 2×10^{12} photons s^{-1} $(100\ mA)^{-1}$ at the P $L_{2,3}$-edge with a resolving power ($E/\Delta E$) better than 3000 with an entrance- and exit-slit setting of 50 µm (Hu *et al.*, 2007). In this study a high-energy grating was used to access the energy range from 100 to 250 eV. P $L_{2,3}$-edge spectra were recorded between 130 and 155 eV with a step size of 0.1 eV and a dwell time of 1 s. The entrance and exit slits were set at 50 µm × 50 µm. The angle between the incident beam and the sample surface was kept constant at 90°. Spectra were recorded in the fluorescence yield mode (FLY) using a microchannel-plate detector and the total electron yield (TEY) mode measuring the sample current with an amperemeter. All spectra were normalized to the intensity of the incident beam (I_0), which was measured simultaneously as the current emitted from a gold mesh located after the last optical elements of the beamline. The absolute energy was calibrated using the Kr $3d$ to $5d$ transition at 91.200 eV and Ar $2p$ to $4s$ line at 244.39 eV (Domke *et al.*, 1992). As the experiments took place over several different measurement periods, the beamline calibration could not be considered as static. Therefore, several reference standards with 'sharp' resonances were measured in two or more experimental runs and the energy calibration was adjusted accordingly. A total of two to three scans were averaged to yield a better signal-to-noise ratio for each compound. To minimize X-ray-induced chemical changes the sample position was adjusted slightly after each scan so the beam hit a 'fresh' sample spot. For a consistent data treatment the background correction was carried out by subtracting an extrapolated linear curve between the first data point and the starting point of the first pre-edge feature using *OriginPro 8* (OriginLab, MA, USA). The non-linear background is possibly caused by other excitations, low-energy electrons and sample charging. A polynomial fit was subtracted to straighten the pre-edge region in front of the first feature. For a better spectral comparison each spectrum was normalized to the peak with maximum intensity in the energy range <140 eV. The corresponding scaling factors are also displayed on the left side of the spectra to allow comparisons of the absolute intensities. All spectra are presented without additional smoothing.

3. Results and discussion

3.1. Spectra of pure P reference compounds

The P $L_{2,3}$-edge XANES spectra exhibited several features, which varied among compounds. The FLY and TEY spectra exhibit similar spectral features but for most compounds features were more clearly resolved in the FLY spectra (Fig. 1). This is in agreement with Kasrai *et al.* (1993), who also reported a better resolution for FLY than for TEY. This finding can be explained by the higher background of the TEY signal which is dominated by low-energy secondary electrons. Furthermore, as TEY measurements are more surface sensitive, and some of the reference compounds studied here were of low conductivity, spectra were affected by surface charging effects. This is an issue for *L*-edge more than for *K*-edge measurements, since the maximum sampling depth of the TEY at the *L*-edge is much lower than at the *K*-edge [Si *L*-edge: TEY, ∼5 nm; FLY, ∼70 nm; Kasrai *et al.* (1996)]. Furthermore, this surface charging occurs particularly when working with intense focused third-generation beamlines. Despite the low FLY yield for light elements, the lower background of the FLY signal results in a better signal-to-background ratio for the FLY than for the TEY signal. As stated above, the FLY detection is rather a bulk than a surface method. However, it should be noted that the FLY signal at the *L*-edge is still very shallow compared with the corresponding *K*-edge signal.

Figs. 2 to 8 show the stacked FLY spectra of various inorganic and organic reference compounds. The features of an $L_{2,3}$-edge spectrum are generally described by two peaks, labeled as (*a*) and (*b*) at the low-energy side. These two peaks are due to transitions from spin-orbit split 2*p* electrons (into the $2p_{3/2}$ and $2p_{1/2}$ levels, which are usually referred to as the L_3- and L_2-edges, respectively) into the first unoccupied 3*s*-like antibonding state. The 2*p* spin-orbit splitting of ∼1 eV is an atomic property and usually insensitive to the chemical environment. A broad peak is observed at about 2 eV higher. This peak has been assigned to transitions to the 3*p*-like antibonding state in the Si *L*-edge spectrum of SiO_2 (Harp *et al.*, 1990). Transitions to these dipole forbidden 3*p* orbitals are possible because they are usually mixed with characters from other elements, such as O and metal. At even higher energy a broad and intense peak owing to 2*p* to 3*d* transitions can be observed at around 147 eV. The energy position of these peaks is sensitive to the molecular symmetry and to the local chemical environment of P, often called the 'shape resonance' (*e.g.* Li *et al.*, 1994).

All energy positions of the most intense resonances are compiled in Table 1. The energy positions of the shoulders were determined by calculating the second derivative. The position and shape of the peaks varied for the different reference compounds. This variation was more pronounced in the 135–140 eV region than in the higher-energy side of the spectrum.

The stacked P $L_{2,3}$-edge spectra of various potassium and aluminium phosphate salts are shown in Fig. 2. The energy positions of peaks (*a*) 136.1 eV, (*b*) 137.1 eV and (*c*) 138.5 eV

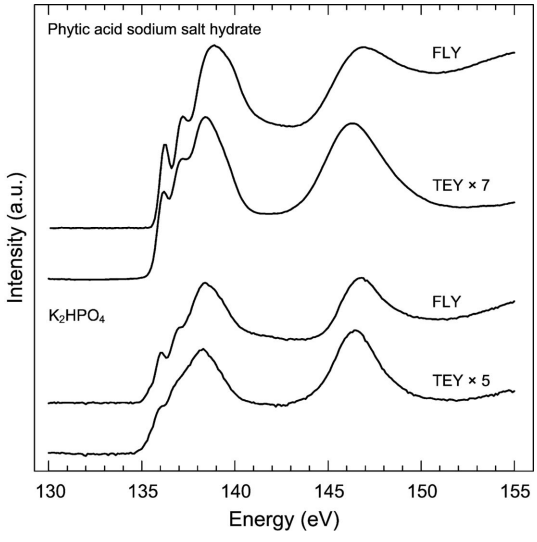

Figure 1
Comparison of the total electron yield (TEY) and fluorescence yield (FLY) spectra for phytic acid sodium salt hydrate and K_2HPO_4. TEY has been multiplied by factors of 7 and 5, respectively.

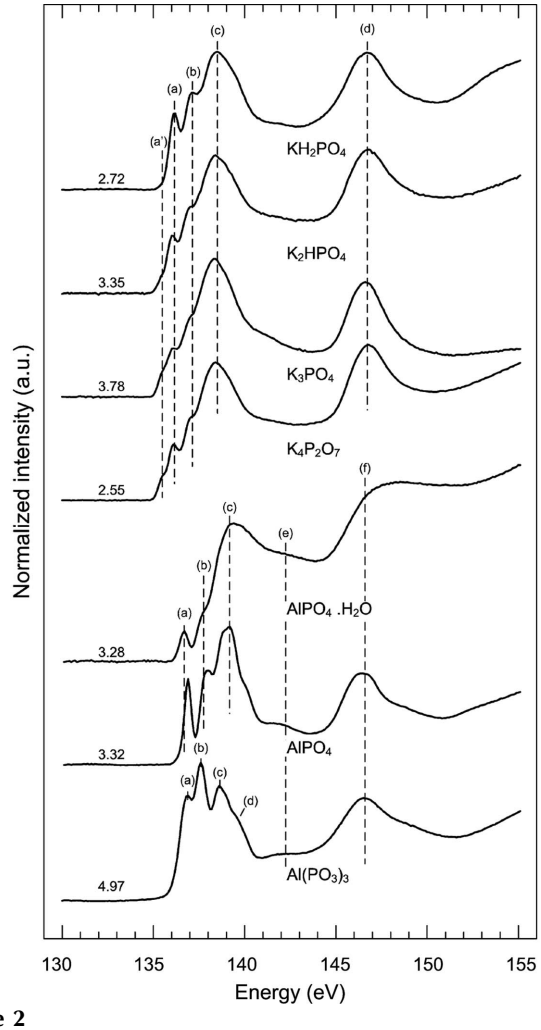

Figure 2
Stacked FLY P $L_{2,3}$-edge XANES spectra of potassium phosphates and aluminium phosphates.

Table 1
Energy position of P $L_{2,3}$-edge XANES spectra of various phosphorus compounds.

sh: shoulder. w: weak. b: broad.

P compound	Formula	CAS	Feature							
			a′	*a*	*b*	*c*	*d*	*e*	*f′*	*f*
Inorganic										
Potassium dihydrogen phosphate	KH_2PO_4	7778-77-0		136.1	137.1	138.5	146.7			
Potassium phosphate dibasic trihydrate	$K_2HPO_4{\cdot}3H_2O$	16788-57-1	135.3^{w,sh}	136.0	136.9^{sh}	138.4	146.8			
Potassium phosphate	K_3PO_4	7778-53-2	135.4^{w,sh}	136.0	136.9^{w,sh}	138.4	146.6			
Potassium pyrophosphate tetrabasic	$K_4P_2O_7$	7320-34-5	135.4^{sh}	136.1	136.9^{sh}	138.4	146.8			
Aluminium phosphate hydrate, light	$AlPO_4{\cdot}H_2O$	66905-65-5		136.7	137.6^{sh}	139.4^{b}		142^{sh}		147.7^{b}
Aluminium phosphate	$AlPO_4$	7784-30-7		136.9	138.0	139.2^{b}	140.1^{sh}	142^{sh}		146.4
Aluminium meta-phosphate	$Al(PO_3)_3$	13776-88-0		136.8	137.6	138.6	139.7^{w,sh}	142^{sh}		146.5
Calcium bis dihydrogen-phosphate mono-hydrate	$Ca(H_2PO_4)_2{\cdot}H_2O$	10031-30-8		136.5	137.4	138.6		142^{w,sh}		146.9
Calcium hydrogen-phosphate dihydrate	$CaHPO_4{\cdot}2H_2O$	7789-77-7		136.4	137.3^{sh}	138.2	138.9^{sh}	141.6^{b}		146.9
Calcium pyrophosphate	$Ca_2P_2O_7$	7790-76-3		136.4	137.3	137.9	138.5^{sh}	141.4^{sh,b}		146.6
α-Tri-calciumphosphate	$Ca_3(PO_4)_2$	7758-87-4		135.9	136.9^{w,sh}	137.9		141.4^{sh,b}		146.7
Magnesium phosphate tribasic octahydrate	$Mg_3(PO_4)_2{\cdot}8H_2O$	13446-23-6		136.3	137.2^{sh}	138.2^{w,sh}	139.2	140^{sh}	146.4^{w,sh}	148.1
Magnesium phosphate dibasic trihydrate	$MgHPO_4{\cdot}3H_2O$	7782-75-4		136.4	137.3^{sh}	138.3^{w,sh}	139.1	140^{w,sh}		147.1
Magnesium pyro-phosphate	$Mg_2P_2O_7$	13446-24-7		136.3	137.2^{sh}	138.2^{w,sh}	139.3			147.4
Iron(III) phosphate tetra-hydrate	$FePO_4{\cdot}4H_2O$	31096-47-6		136.5	141.4^{b}		147.8			
Sodium phosphate mono-basic dihydrogen	$NaH_2PO_4{\cdot}2H_2O$	13472-35-0		136.2	137.2	138.9	146.8			
Sodium phosphate dibasic dihydrate	$Na_2HPO_4{\cdot}2H_2O$	10028-24-7	135.6^{sh}	136.3	137.1^{w,sh}	138.9	146.4			
Sodium pyrophosphate decahydrate	$Na_4P_2O_7{\cdot}10H_2O$	13472-36-1	135.5^{sh}	136.1^{w,sh}	136.8^{w,sh}	138.7	146.7			
Sodium triphosphate pentabasic	$Na_5P_3O_{10}$	7758-29-4		136.3	137.1	138.8	146.7			
Sodium hexameta-phosphate	$(NaPO_3)_6$	10124-56-8		136.2	137.1	138.6^{b}	146.9			
Ammonium phosphate dibasic	$NH_4H_2PO_4$	7783-28-0		136.3^{sh}	137.4	138.7	146.8			
Ammonium dihydrogen-phosphate	$(NH_4)_2HPO_4$	7722-76-1		136.2^{sh}	137.3	138.6	146.7			
Zinc phosphate hydrate	$Zn_3(PO_4)_2{\cdot}xH_2O$			135.3	136.2^{sh}	139.1	147.1			
Organic										
O-Phosphorylethanol-amine		1071-23-4		136.1^{sh}	137.2	138.4	146.7			
2-Aminoethylphosphonic acid		2041-14-7		136.0^{w,sh}	137.2	138.3	146.7			
N-(Phosphonomethyl)-glycine		1071-83-6		136.0^{sh}	137.0	138.3	146.7			
β-Glycerol phosphate disodium salt penta-hydrate		13408-09-8		136.2	137.1^{sh}	139.2	147.1			
L-α-Phosphatidyl choline		8002-43-5		136.2	137.0^{sh}	139.0	146.9^{b}			
L-α-Phosphatidylethanol-amine		39382-08-6		136.0	137.0^{sh}	139.0	147.0^{b}			
Asolectin		MFCD00146015		136.2	137.1^{sh}	138.9	147.0			
Adenosine 5′-monopho-sphate disodium salt		4578-31-8		136.1	137.0^{w,sh}	138.8	146.6			
Adenosine 5′-diphosphate disodium salt		16178-48-6		136.1	137.1	138.6	146.5			
Adenosine 5′-tri-phosphate disodium salt hydrate		34369-07-8		136.1	137.0	138.5	146.6			
Cytidine-5′-triphosphoric acid disodium salt		18423-42-2		136.1	137.1	138.7	146.6			

Table 1 (continued)

P compound	Formula	CAS	Feature							
			a′	*a*	*b*	*c*	*d*	*e*	*f′*	*f*
Inosine 5′-monophosphate disodium salt		352195-40-5		136.1	137.0[sh]	138.6	146.4			
Ribonucleic acid				136.1	137.1[sh]	138.9	147.0			
Phytic acid sodium salt hydrate		14306-25-3		136.2	137.2	138.9	147.0			
Phytic acid calcium salt		23183-60-0		136.6	137.5	138.5	146.5			
Diethyl phosphoramidate		1068-21-9		136.4[w,sh]	137.3[w,sh]	139.1	147.3[b]			
Imidodiphosphate sodium salt		26039-10-1		136.2	137.1[sh]	139.4	147.2[b]			
Sodium creatine phosphate dibasic tetrahydrate		922-32-7		136.2	137.0[sh]	138.8	146.8			
Sodium phenyl phosphate dibasic dihydrate		66778-08-3	135.5[sh]	136.2[w,sh]	137.0[w,sh]	138.7	146.6			
Diphenyl phosphate		838-85-7		136.4[sh]	137.4	138.8	146.3			
Triphenyl phosphate		115-86-6		136.5[sh]	137.5	138.9	146.5			
Phenylphosphonic acid		1571-33-1		134.6[w,sh]		136.5[sh]	137.4	138.5		146.7[b]
Phenylphosphinic acid		1779-48-2		133.8[w,sh]	134.7[w,sh]	136.3[sh]	137.1	138.3[sh]		146.3[b]
Minerals										
Apatite				136.3	137.2	137.9	138.6	141.4[sh]		146.7
Phosphorite				136.4	137.3	138.0	138.7	141.4[sh]		146.7
Triphylin				136.3[sh]	137.2[w,sh]	139.3	147.1			
Triploidite				136.3[w,sh]	137.1[w,sh]	139.2	146.8			
Pyromorphite			135.4[b]	136.5[w,sh]	137.4[w,sh]	139.5	140.3	147.5		
Amblygonite				137.2	138.0	138.8[sh]	139.2	140.3[w,sh]		147.1
Lazulite				137.1	138.0	138.7[sh]	139.3	140.2[sh]		147.2
Variscite				136.8	137.7[sh]	139.0	142.0[w,sh]	147		
Wavellite				136.6	137.5[sh]	139.0	142.1[w,sh]	146.7		
Vivianite				136.8	139.1		147.7			

for all four potassium phosphates were almost identical but their relative intensities varied. The absolute intensity of the broad peak (*c*) increased in the order $KH_2PO_4 < K_2HPO_4 < K_3PO_4 < K_4P_2O_7$. By contrast the relative intensities of peaks (*a*) and (*b*) decreased in the order $KH_2PO_4 > K_2HPO_4 = K_4P_2O_7 > K_3PO_4$. Furthermore, a weak shoulder (*a′*) appeared on the low-energy side of peak (*a*) and became more pronounced with increasing number of potassium atoms in the salts. The origin of this shoulder is still unknown. The overall shape of the $K_4P_2O_7$ spectrum was quite similar to the spectrum of K_2HPO_4. This similarity was surprising since these compounds have quite different structures (PO_4^{3-} *versus* $P_2O_7^{4-}$). The only spectral difference was a slightly more developed shoulder in front of peak (*a*) in the $K_4P_2O_7$ than in the K_2HPO_4 spectrum. Peak (*d*) appeared in all potassium phosphates around 146.7 eV.

The peaks (*a*), (*b*) and (*c*) in the spectra of the aluminium phosphates and metaphosphates appeared at higher energy than in the spectra of the potassium phosphates. On the other hand, peak (*f*) remained at almost the same energy position at ∼147 eV in the Al phosphate spectra. However, an additional shoulder was resolved at the high-energy side of peak (*f*) in the spectra of $AlPO_4$ and $Al(PO_3)_3$. This shoulder was not resolved in the spectrum of $AlPO_4{\cdot}H_2O$ but peak (*f*) was broader than in the former spectra. In the spectrum of $AlPO_4{\cdot}H_2O$ peak (*a*) appeared at 136.7 eV and peak (*b*) was only resolved as a shoulder at 137.6 eV. Peaks (*a*) and (*b*) were slightly shifted to higher energies of 136.9 eV and 138 eV in the spectrum of $AlPO_4$ and the relative intensities of both peaks increased. Furthermore, in the spectrum of $AlPO_4{\cdot}H_2O$ peak (*c*) at 139.4 eV was broader than in the two other Al phosphates. In the spectrum of $AlPO_4$ peak (*c*) at 139.2 eV showed a weak shoulder at 138.8 eV and a strong shoulder (*d*) at 140.1 eV. Moreover, shoulder (*e*) at around 142 eV was better resolved in the spectrum of $AlPO_4$ than in the spectrum of $AlPO_4{\cdot}H_2O$. These differences reflect the different local environments of the P atom owing to the absence or presence of crystal water.

Different from $AlPO_4$ and $AlPO_4{\cdot}H_2O$ the P atom in $Al(PO_3)_3$ is coordinated to three oxygen atoms involving two double bonds. This local environment of the P atom was reflected by the XANES spectrum. Although peaks (*a*) and (*b*) appeared at the same energy position as in the other Al phosphates, their relative intensity was much higher. Peak (*c*) appeared at lower energy (138.6 eV). This peak seemed to be a convolution of possibly three weakly resolved peaks [138.6 eV, ∼139 eV and (*d*) 139.7 eV], similar to $AlPO_4$. Furthermore, feature (*e*) was also resolved at around 142 eV and the shape of resonance (*f*) at 146.5 eV also showed a shoulder at the high-energy side.

Fig. 3 shows the stacked P $L_{2,3}$-edge XANES spectra of four different Ca phosphates. The spin-orbit doublet appeared at the same energy positions (*a*) at 136.4 eV and (*b*) at 137.3 eV in the spectra of $Ca(H_2PO_4)_2{\cdot}H_2O$, $CaHPO_4{\cdot}2H_2O$ and $Ca_2P_2O_7$. The relative intensity of peak (*a*) increased in the order $CaHPO_4{\cdot}2H_2O < Ca(H_2PO_4)_2{\cdot}H_2O < Ca_2P_2O_7$. The

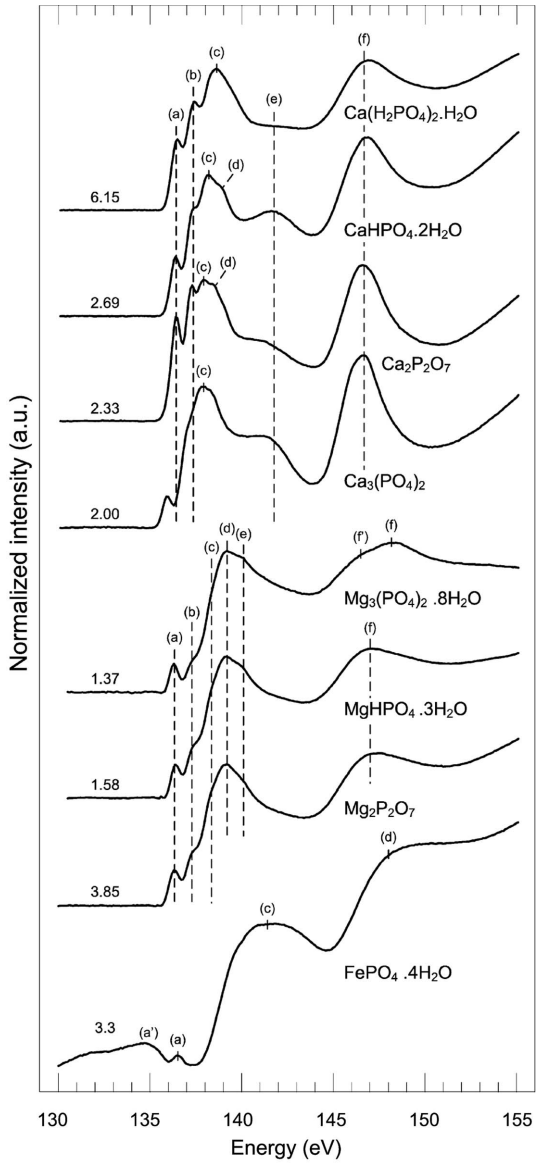

Figure 3
Stacked FLY P $L_{2,3}$-edge XANES spectra of calcium phosphates, magnesium phosphates and iron phosphate.

relative intensity of peak (*b*) was the same in the spectra of $Ca(H_2PO_4)_2{\cdot}H_2O$ and $CaHPO_4{\cdot}2H_2O$. However, this peak was better resolved in $Ca(H_2PO_4)_2{\cdot}H_2O$ than in $CaHPO_4{\cdot}2H_2O$. The relative intensity of peak (*b*) was higher in the spectrum of $Ca_2P_2O_7$ as in the two Ca phosphates mentioned above. In the spectrum of $Ca_3(PO_4)_2$ the doublet was shifted to lower energy and appeared at 135.9 eV (*a*) and 136.9 eV (*b*). The relative intensity of peak (*a*) was much lower than in the other Ca phosphates and peak (*b*) was only resolved as a shoulder. The absolute intensity of peak (*c*) was larger by factors up to two in the spectrum of $Ca(H_2PO_4)_2{\cdot}H_2O$ than in the other Ca phosphates as indicated by the scaling factors on the left side of the spectra. Peak (*c*) was observed as a broad peak at 138.6 eV in the spectrum of $Ca(H_2PO_4)_2{\cdot}H_2O$. In the spectra of $CaHPO_4{\cdot}2H_2O$ and CaP_2O_7 this broad peak was split into two features (*c*) at 138.2 eV and (*d*) at 138.9 eV for $CaHPO_4{\cdot}2H_2O$, and features (*c*) at 137.9 eV and (*d*) 138.5 eV for CaP_2O_7. All Ca phosphates in Fig. 3 showed a shoulder (*e*) at the high-energy side of peak (*c*). This seems to be a distinguishing feature for Ca phosphates only, and can possibly be explained by transitions of P 2*p* to Ca 3*d* empty orbitals. The shape resonance peak (*f*) appeared in all Ca phosphates at around 146.9 eV. Our spectra of $Ca_2P_2O_7$ and $Ca_3(PO_4)_2$ confirmed Kasrai *et al.* (1999) and Varlot *et al.* (2001) but the $Ca_2P_2O_7$ spectrum in Fig. 3 was less noisy then those published by Varlot *et al.* (2001).

The XANES spectra of the three Mg phosphates $Mg_3(PO_4)_2{\cdot}8H_2O$, $MgHPO_4{\cdot}3H_2O$ and $Mg_2P_2O_7$ had a very similar overall shape (Fig. 3). The spin-orbit doublet peaks appeared at the same energy positions of 136.3 eV (*a*) and 137.2 eV (*b*) in all Mg phosphates. The relative intensities of both peaks were almost the same in the spectra of $MgHPO_4{\cdot}3H_2O$ and $Mg_2P_2O_7$ whereas both peaks, particularly (*b*), were less intense in the spectrum of $Mg_3(PO_4)_2{\cdot}8H_2O$. Peak (*d*) appeared in all three spectra at around 139.2 eV. However, the absolute intensity of peak (*d*) was larger by a factor up to two in $Mg_2P_2O_7$ than in the other Mg phosphates. Furthermore, a weak shoulder (*c*) at around 138.2 eV at the low-energy side of peak (*d*) appeared in all spectra of Mg phosphates, and was most pronounced in the spectrum of $Mg_2P_2O_7$. Another shoulder (*e*) was weakly resolved at around 140 eV and decreased in the order $Mg_3(PO_4)_2{\cdot}8H_2O$ > $MgHPO_4{\cdot}3H_2O$ > $Mg_2P_2O_7$. The shape resonance (*f*) appeared at around 147.2 eV. In the spectrum of $Mg_3(PO_4)_2{\cdot}8H_2O$ the shape resonance seemed to be resolved into a main resonance at around 148.1 eV and a weak shoulder (*f*′) at around 146.4 eV.

The spectrum of $FePO_4{\cdot}4H_2O$ was dominated by a broad peak (*c*) at around 141.4 eV. Interestingly in this spectrum only peak (*a*) of the spin-orbit doublet was resolved with low intensity at 136.5 eV. Furthermore, a broad low-energy peak (*a*′) appeared at around 134.8 eV. This peak was previously shown in P $L_{2,3}$-edge spectra of $FePO_4$ (Kasrai *et al.*, 1999; Najman *et al.*, 2002). By contrast, the $FePO_4$ spectra published by Yin *et al.* (1997) did not show this peak. Peak (*a*′) might be attributed to a P 2*p* electron transition into unoccupied states with partial 3*d* character formed by hybridization of Fe(3*d*), O(2*p*) and P(3*p*) orbitals. A similar distinctive low-energy feature also occurs in Fe phosphate spectra at the P *K*-edge (Franke & Hormes, 1995). In contrast to our results, both peaks (*a*) and (*b*) were resolved in the spectra of $FePO_4$ published by Yin *et al.* (1997) and Najman *et al.* (2002). The reason for these spectral differences might be an alteration of the geometrical and chemical environment of the phosphorus owing to crystal water as already shown for the difference between $AlPO_4$ and $AlPO_4{\cdot}H_2O$.

All XANES spectra of various Na phosphates showed the first spin-orbit doublet at almost the same energy position: peak (*a*) at around 136.2 eV and peak (*b*) at around 137.1 eV (Fig. 4). The relative intensities of peaks (*a*) and (*b*) varied significantly among the Na phosphates. In the spectra of $Na_2H_2PO_4{\cdot}2H_2O$, $Na_5P_3O_{10}$ and $(NaPO_3)_6$ peaks (*a*) and (*b*) were well resolved from peak (*c*). These features were resolved only as shoulders in the spectra of the other Na

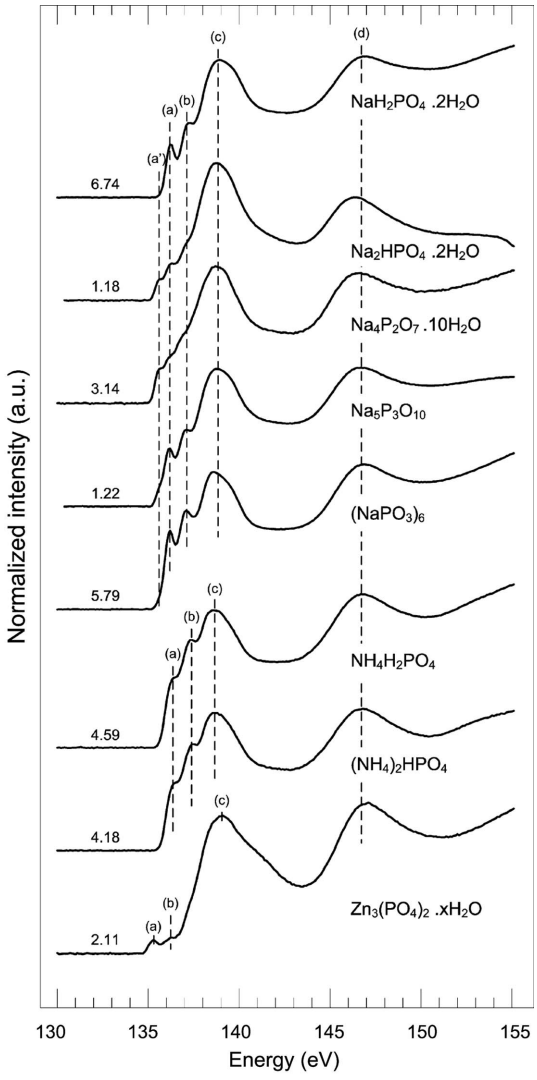

Figure 4
Stacked FLY P $L_{2,3}$-edge XANES spectra of sodium phosphates, ammonium phosphates and zinc phosphate.

phosphates. Furthermore, a more or less weak additional shoulder (a') appeared at around 135.5 eV in the spectra of $NaHPO_4{\cdot}2H_2O$, $Na_4P_2O_7{\cdot}10H_2O$ and $Na_3PO_3S{\cdot}12H_2O$. The broad peak (c) appeared in the range 138.6 eV to 139 eV. Peak (c) seems to be always a convolution of several unresolved peaks. This was particularly obvious in the spectrum of $(NaPO_3)_6$ where peak (c) was more asymmetric owing to the shoulder at the high-energy side than in the other spectra of Na phosphates in Fig. 4. The shape resonance (d) of the Na phosphates was at around 146.8 eV. This peak was slightly shifted towards lower energy (−0.4 eV) in the spectrum of $Na_2HPO_4{\cdot}2H_2O$. Fig. 4 shows a pronounced difference between the spectra of $NaH_2PO_4{\cdot}2H_2O$ and $NaHPO_4{\cdot}2H_2O$ although only one of the H atoms was substituted by another Na atom. However, this substitution altered the local environment of the P atom and thus may explain the difference in the spectral features.

The increasing relative intensity of peak (a) and (b) in the order $Na_5P_3O_{10}$ < $Na_4P_2O_7{\cdot}10H_2O$ ≪ $(NaPO_3)_6$ confirmed Yin *et al.* (1995) who reported increases in the relative intensity of the low-energy spin-orbit doublet with increasing chain length of different Na polyphosphates. However, Yin *et al.* (1995) did not report a shoulder (a') preceding peak (a) in their spectrum of $Na_4P_2O_7$. This is explained by the alteration of the symmetry by the crystal water in our $Na_4P_2O_7{\cdot}10H_2O$ spectrum.

In the spectra of the two ammonium phosphates in Fig. 4 the peaks (a) at 136.3 eV, (b) at 137.4 and (d) at 138.7 eV appeared at almost the same energy position. Furthermore, they are also similar in absolute intensities. Our spectrum of $(NH_4)_2HPO_4$ agreed well with that published by Najman *et al.* (2002).

Finally, the energy positions of peaks (a) at 135.3 eV, (b) at 136.2 eV, (c) at 139.1 eV and (d) at 147.1 eV in the spectrum of Zn phosphate (Fig. 4) were in good agreement with Yin *et al.* (1997) and Fuller *et al.* (1998) if we shift their energy scale by +0.8 eV and +0.7 eV, respectively.

The P $L_{2,3}$-edge XANES spectra of organic phosphorus compounds were all dominated by three peaks (Fig. 5). In the

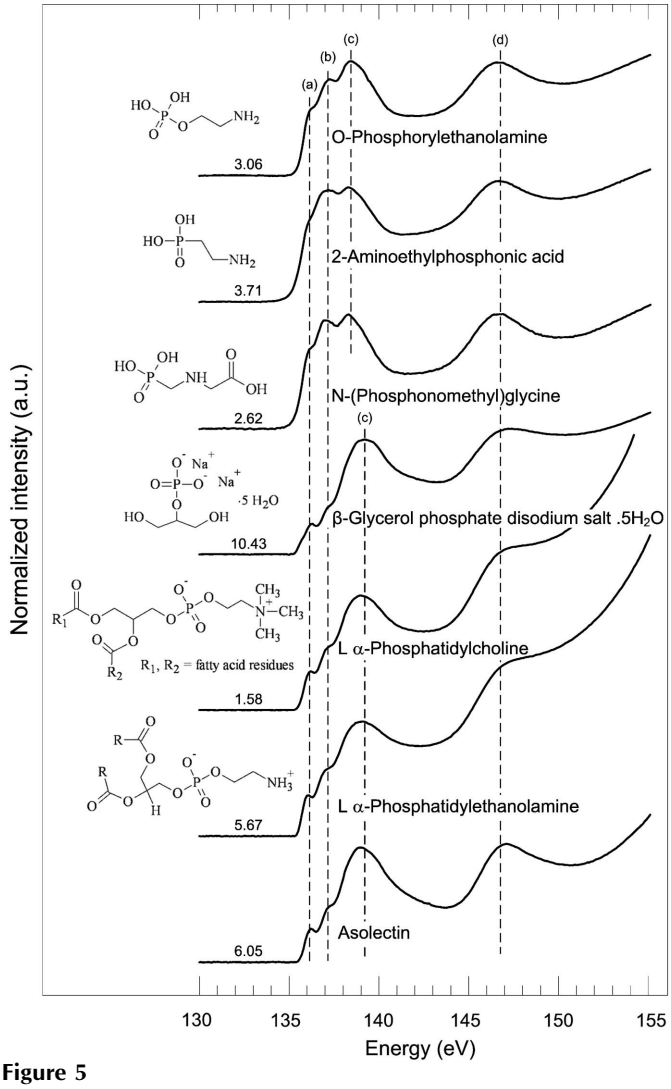

Figure 5
Stacked FLY P $L_{2,3}$-edge XANES spectra of various organic P compounds.

spectra of *O*-phosphorylethanolamine and 2-amidoethylphosphonic acid the peaks (*a*) 136.1 eV, (*b*) 137.2 and (*c*) 138.4 eV appeared at the same energy position. Only in *N*-(phosphonomethyl)glycine peak (*b*) appeared already at 137 eV. This concordance was surprising since 2-amidoethylphosphonic acid and *N*-(phosphonomethyl)glycine contain P(+III) whereas *O*-phosphorylethanolamine contains P(+V). This difference in valence of the P atoms was reflected on the P *K*-edge by an energy shift of −0.6 eV in the white-line position of 2-amidoethylphosphonic acid (Brandes *et al.*, 2007). There are two possible explanations for the absence of such an energy shift at the $L_{2,3}$-edge: (i) the oxidation state of the P atom in these compounds does not always have the same impact on the spectral features in the P $L_{2,3}$-edge as in the P *K*-edge spectra; (ii) X-rays led to a further oxidation of P within theses compounds. However, the spectra differed in the relative intensity of the spin-orbit doublet peaks (*a*) and (*b*). This doublet had a lower relative intensity in the spectra of *O*-phosphorylethanolamine than in 2-amidoethylphosphonic acid and *N*-(phosphonomethyl)glycine where the intensity of peaks (*b*) and (*c*) was almost equal. The relative intensities in both P(+III)-containing compounds were similar even though peaks (*a*) and (*b*) were better resolved in the spectrum of *N*-(phosphonomethyl)glycine. By contrast, the peaks (*a*) 136.2 eV and (*b*) 137 eV were much lower in relative intensity in all other spectra in Fig. 5. In the spectrum of L-α-phosphatidylethanolamine peak (*a*) was slightly shifted by −0.2 eV. The broad peak (*c*) occurred in the three phospholipids and β-glycerol phosphate disodium salt pentahydrate at around 139 eV and the absolute intensity of peak (*c*) increased in the order L-α-phosphatidyl choline ≪ L-α-phosphatidylethanolamine < asolectin.

In all spectra of nucleotides and for ribonucleic acid the peaks (*a*) and (*b*) were at the same energy position of 136.1 eV and 137 eV, respectively (Fig. 6). This disagreed with Yin *et al.* (1997) who reported that peaks (*a*) and (*b*) shifted to higher energy with increasing P chain length in sodium polyphosphates. However, we also found a chain length effect on the relative intensities of peaks (*a*) and (*b*) in the spectra of adenosine 5′-monophosphate disodium salt (AMP), adenosine 5′-diphosphate disodium salt (ADP) and adenosine 5′-triphosphate disodium salt hydrate (ATP), confirming Yin *et al.* (1997) in this respect. In these spectra the relative intensities of the low spin-orbit doublet increased in the order AMP ($n = 1$) < ADP ($n = 2$) < ATP ($n = 3$). The fact that the relative intensity of peaks (*a*) and (*b*) in cytidine-5′-triphosphoric acid disodium salt ($n = 3$) was lower than in ATP and the relative intensity in inosine 5′-monophosphate disodium salt ($n = 1$) higher than in AMP indicate that the relative intensity of the spin-orbit doublet may also be influenced by other factors than the chain length of the polyphosphate. All nucleotide spectra were dominated by the broad peak (*c*) in the energy range 138.5 to 138.8 eV. The position of peak (*d*) was constant in all nucleotides. Finally, Fig. 6 shows the spectra of phytic acid sodium salt hydrate and phytic acid calcium salt. Relative to phytic acid sodium salt hydrate, all the peaks in the spectrum of phytic acid calcium salt were shifted: (*a*) +0.4 eV, (*b*) +0.3 eV, (*c*) −0.4 eV, (*d*) −0.5 eV. Furthermore, the relative intensities of peaks (*a*) and (*b*) were much lower for the phytic acid sodium salt hydrate and peak (*c*) was broader than in the spectrum of phytic acid calcium salt. This difference in the phytic acid salts was more pronounced than in P *K*-edge measurements (He *et al.*, 2007), indicating that XANES at the P $L_{2,3}$-edge may be more sensitive to distinguish between different phytic acid salts than P *K*-edge XANES.

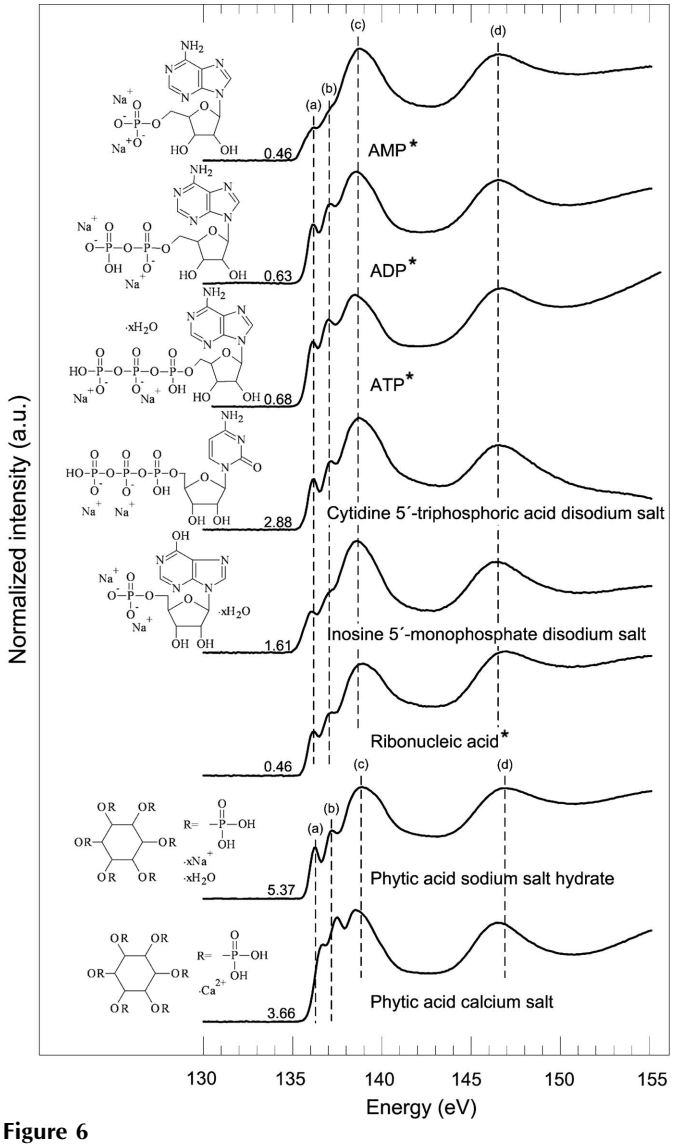

Figure 6
Stacked FLY P $L_{2,3}$-edge XANES spectra of nucleotides, RNA and phytic acid salts. Compounds labeled with an asterisk (*) were measured using a 100 μm × 100 μm slit.

The spectra of diethyl phosphoramidate, imidodiphosphate sodium salt and sodium creatine phosphate, which contain P directly bonded to an N atom, showed three main features (Fig. 7). The spin-orbit doublet peaks (*a*) and (*b*) appeared at 136.2 eV and 137 eV in the spectra of imidodiphosphate sodium salt and sodium creatine phosphate. The doublet was resolved as weak shoulders only and slightly shifted (+0.2 eV) in the case of diethyl phosphoramidate. In the spectrum of sodium phenyl phosphate dibasic dihydrate the peaks (*a*) and

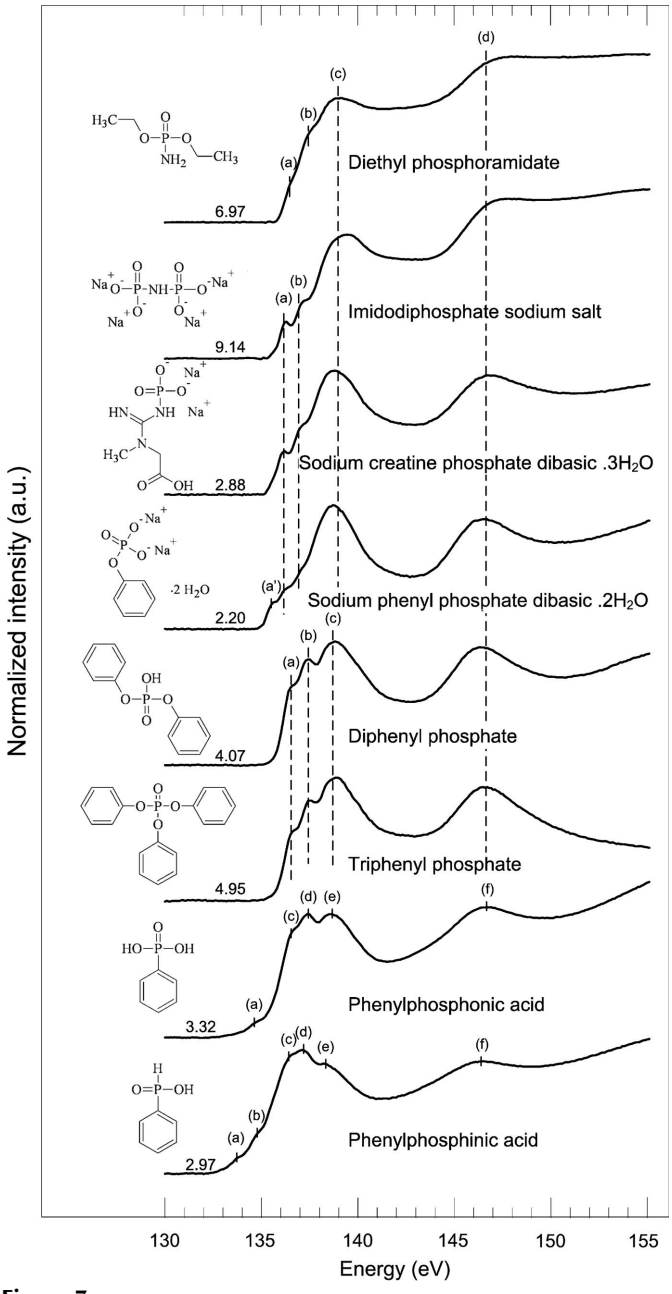

Figure 7
Stacked FLY P $L_{2,3}$-edge XANES spectra of organic P compounds with a N atom or phenol group directly attached to the P atom and one or more phenol groups attached to the phosphate tetrahedron.

(*b*) appeared at 136.2 eV and 137 eV. Furthermore, a shoulder (*a*′) was resolved at 135.5 eV. The energy positions of features (*a*′), (*c*) and (*b*) were almost the same as in the structurally similar $Na_2HPO_4{\cdot}2H_2O$ (Fig. 3). The slightly higher relative intensity of peaks (*a*′), (*a*) and (*b*) as well as the modified curve shape above 142 eV may result from the additional phenol group bonded to one of the O atoms in the phosphate tetrahedron in sodium phenyl phosphate dibasic dihydrate.

Obviously, the energy position of the spin-orbit doublet as well as peak (*c*) remained unchanged irrespective of two or three phenol groups bonded to the phosphate tetrahedron. Solely the relative intensities of peaks (*a*) and (*b*) were slightly higher and peak (*b*) somewhat better resolved in the spectrum of diphenyl compared with triphenyl phosphate. The differences in the spectra of sodium phenyl phosphate dibasic dihydrate and diphenyl triphenyl phosphates cannot be explained exclusively by the additional phenyl groups in the latter but must be caused also by the different structure and crystal water of sodium phenyl phosphate dibasic dihydrate.

The spectra of phenylphosphonic acid and phenylphosphinic acid were completely different from those shown above as they had features at <135.5 eV (Fig. 7). We tentatively assign peak (*a*) 134.6 eV in the spectrum of phenylphosphonic acid to the first peak of the low-energy spin-orbit doublet corresponding to the transition from $2p_{3/2}$ into the first unoccupied antibonding orbital. The second peak of this doublet was not resolved in this spectrum, but the curve shape indicated another peak. A weak feature in the second derivative at around 135.5 eV seemed to corroborate this. This would result in a difference of ∼0.9 eV between peaks (*a*) and (*b*) which agreed with the spectra of the other P compounds. In phenylphosphinic acid both parts of the doublet were resolved as shoulders at 133.8 eV (*a*) and 134.7 eV (*b*). The shift of the spin-orbit doublet towards lower energy might be explained by the lower oxidation state of P in both compounds. This shift was higher for phenylphosphinic acid containing P(−I) than for phenylphosphonic acid containing P(+III). The difference in the energy position of the main peak was measured for both compounds at the P *K*-edge (Brandes *et al.*, 2007). To test whether there is a general trend for the P $L_{2,3}$-edge depending on oxidation state, more reference compounds with oxidation state lower than P(+V) must be measured since the P(+III) containing 2-amidoethylphosphonic acid and *N*-(phosphonomethyl)glycine (Fig. 5) did not show corresponding shifts in the energy range. Furthermore, phenylphosphonic acid and phenylphosphinic acid exhibited three other peaks: (*c*) 136.5 eV/136.3 eV, (*d*) 137.4 eV/137.1 eV and (*e*) 138.5 eV/138.3 eV. In both spectra peak (*d*) was the most intense feature.

3.2. Spectra of P minerals from geological sources

Fig. 8 shows the P $L_{2,3}$-edge XANES spectra of various P(+V)-bearing minerals and their general formula (Rösler, 1991). The spectra of apatite and phosphorite were very similar as could be expected because phosphorite consists mainly of cryptocrystalline fluorapatite (Rösler, 1991). Since both minerals were Ca phosphates the spectral features matched with the Ca phosphates in Fig. 3, particularly the strong shoulder (*e*) at around 141.4 eV. The energy position of peaks (*a*), (*b*), (*c*), as well as the relative intensities, were more similar to $Ca_2P_2O_7$ than to the other Ca phosphates shown in Fig. 3. In the spectra of triphylite and tripolidite the spin-orbit doublet appeared at almost the same energy position as in apatite and phosphorite: (*a*) at 136.3 eV and (*b*) at 137.2 eV. However, the spin-orbit doublet was less intense in triphylite and tripolidite than in the above spectra. Furthermore, only one very broad and asymmetric peak (*c*) was resolved. Pyromorphite showed a broad low-energy feature (*a*′) at 135.4 eV

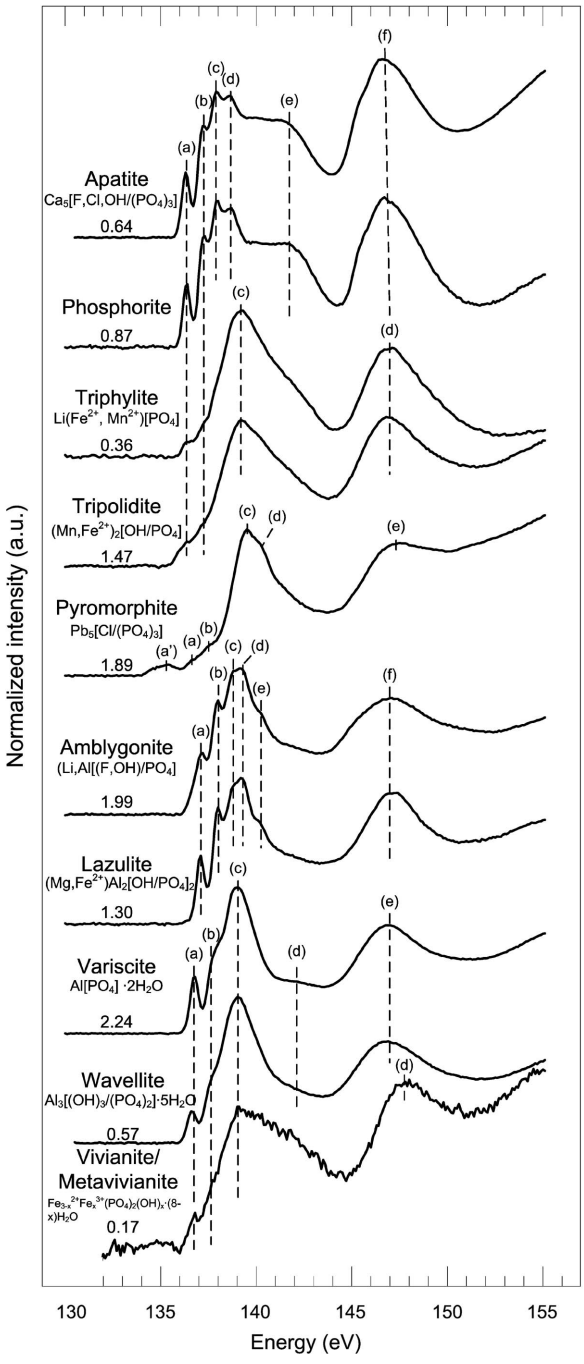

Figure 8
Stacked FLY P $L_{2,3}$-edge XANES spectra of various geological P minerals.

which might be a characteristic low-energy feature for Pb-containing phosphates. In this spectrum peaks (*a*) and (*b*) were only poorly resolved and tentatively assigned to the spin-orbit doublet arising from the transition of the $2p_{3/2}$ and $2p_{1/2}$ levels to the first *s*-like unoccupied antibonding orbital. The spectra of amblygonite and lazulite were quite similar despite their different elemental composition. However, the spin orbit-doublet peaks (*a*) and (*b*) were better resolved in lazulite than in amblygonite. The spectrum of the Al phosphate variscite was very similar to the spectra of the Al reference compounds in Fig. 2. The peaks (*a*) and (*b*) in the spectrum of variscite resembled the spectrum of $AlPO_4{\cdot}H_2O$ but the shape of peak (*c*) was different. In the spectra of wavellite and variscite peak (*c*) appeared at the same energy position at 139. eV. However, peaks (*a*) and (*b*) were slightly higher in energy in the latter spectrum. Shoulder (*e*), more or less intensive in all Al phosphates in Fig. 2, was also resolved at 142 eV in the spectrum of variscite. This shoulder was only weak for the wavellite. The poor signal-to-noise ratio in the spectrum of metavivianite is explained by the lower P concentration than in the other P minerals. Peak (*a*) appeared at 136.8 eV which was slightly higher in energy than in $FePO_4{\cdot}4H_2O$. Again the second peak of the spin-orbit doublet (*b*) could not be resolved. Furthermore, peak (*c*) at around 139.1 eV was similarly broad as in the spectrum of $FePO_4{\cdot}4H_2O$. However, the broad low-energy feature was not resolved in the mineral which is an effect of the poor signal-to-noise ratio.

3.3. X-ray beam impact on the samples and spectral alterations

In order to examine possible X-ray-induced chemical changes and spectral modifications, we compared three consecutive scans of ATP taken at the same sample spot (slit size 100 µm × 100 µm) (Fig. 9*a*). The low-energy spin-orbit doublet (*a*) and (*b*) became less well resolved and clearly increased in relative intensity [normalized to peak (*c*)] from scan one to scan two. In the third scan the intensity of peak (*b*) was almost equal to that of peak (*c*). However, the energy position of peaks (*a*) and (*b*) remained unaffected. By contrast, there was a slight change in the energy position of peak (*c*) by about −0.1 eV with each scan. Along with this change the shape of peak (*c*) became narrower but peak (*d*) remained unaffected.

The slit size setting can be used to tune the overall energy transferred to the sample appropriate to the sample. In order to investigate the effect of the slit size, five consecutive scans of AMP were recorded each time at slit sizes of 50 × 50 µm and 100 × 100 µm. For a better comparison of the relative intensities each spectrum was normalized to the maximum of peak (*c*) (Fig. 9*b*). Fig. 9(*b*) shows that spectral changes were observed for both slit settings with increasing scan number. Furthermore, the change in shape and the shift in the energy position of peak (*c*) followed the same trend in both slit settings. However, the increases in relative intensities of peaks (*a*) and (*b*) between consecutive scans were smaller for the 50 × 50 µm slit size than for the wider slit setting. Changing the slit size reduces the total amount of photons hiding the samples but the brightness, *i.e.* the number of photons per unit area, is not affected by the slit size. The observed difference between both slit settings (Fig. 9*a*) might be explained by the higher amount of energy transferred to the sample through the wider slit, accelerating decomposition-related processes, *e.g.* free-radical formation. To the best of our knowledge, X-ray-induced spectral modifications on the P $L_{2,3}$-edge have not been reported in the literature so far. One reason might be

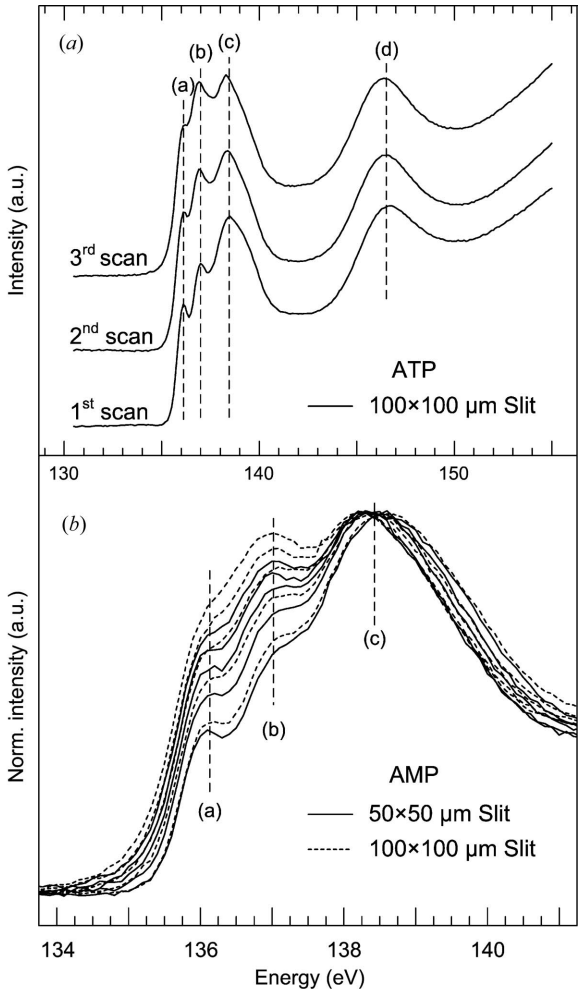

Figure 9
Stacked FLY P $L_{2,3}$-edge XANES spectra of three consecutive scans of ATP showing the spectral changes during X-ray exposure (*a*), and comparison of different slit size settings and their effect on spectra in the zoomed section of five consecutive scans of AMP (*b*).

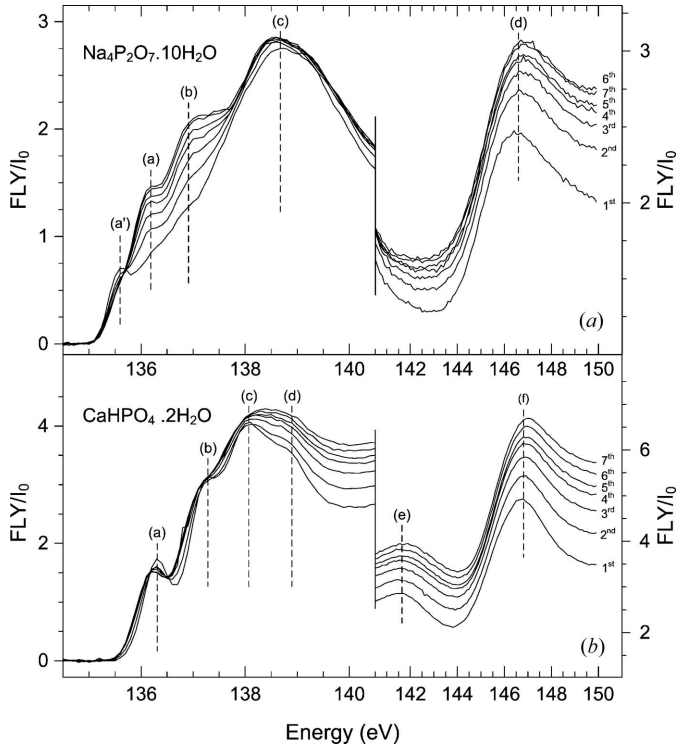

Figure 10
Stacked FLY P $L_{2,3}$-edge XANES spectra of seven consecutive scans of (*a*) $Na_4P_2O_7{\cdot}10H_2O$ and (*b*) $CaHPO_4{\cdot}2H_2O$.

the use of less bright second-generation beamlines so far, whereas the present study was carried out at a third-generation beamline which is characterized by a much higher brightness. A bright source is needed to obtain a P $L_{2,3}$-edge spectrum with sufficient signal-to-noise ratio from samples with low P concentration. It cannot be excluded that X-ray radiation of such a bright source can damage certain compounds during the first scan. However, it can be assumed that the same energy transferred to the sample causes the same radiation damage of a compound irrespective of whether it is pure or in a mixture with other compounds in a real sample. Therefore, spectra of reference compounds with damage-derived features also have a diagnostic value for samples of unknown composition.

The type of decomposition products from ATP and AMP remained unclear. One possible explanation could be the formation of longer polyphosphate chains which increased the relative intensity of the low-energy spin-orbit doublet (*a*) and (*b*).

Consecutive scans of two further compounds, $Na_4P_2O_7{\cdot}10H_2O$ and $CaHPO_4{\cdot}2H_2O$, were recorded with the 50 µm × 50 µm slit size setting (Fig. 10). The intensity of feature (*a*′) rapidly decreased with increasing scan number in Fig. 10(*a*). By contrast, features (*a*) and (*b*) increased in intensity and became more pronounced. The fact that peaks (*a*) and (*b*) formed a broader feature with increasing scan number suggested that several products with slightly different positions for (*a*) and (*b*) were formed under the X-ray impact. Furthermore, peak (*c*) was very slightly shifted towards lower energy but the increase in intensity was small. However, the energy position of peak (*d*) remained constant but the intensity increased with the scan number. It is obvious from Fig. 10(*a*) that the difference in the intensities of features (*a*) to (*d*) between two consecutive scans decreased with increasing scan number. Whereas peaks (*a*′) and (*c*) did not change much after the third scan, peaks (*a*), (*b*) and (*d*) continued to increase. However, after the sixth scan these changes were only marginal too. This indicated that dose- or time-dependent processes may have resulted a quasi-steady state.

The seven consecutive scans of $CaHPO_4{\cdot}2H_2O$ (Fig. 10*b*) showed that radiation-induced spectral modifications were not only a property of polyphosphates. Except for peak (*a*) all features in the spectra of $CaHPO_4{\cdot}2H_2O$ increased in intensity with consecutive scans. Again, this increase followed the same trend as in $NaP_2O_7{\cdot}10H_2O$ although being more intensive at the beginning and less pronounced later. Although features (*a*), (*b*) and (*c*) seemed to be constant during the last three

scans, it remains open whether more scans would result in further increases of peaks (*d*) to (*e*). However, the X-ray-induced processes leading to the observed spectral changes (Fig. 9 and 10) are still unknown.

4. Conclusions

Until now the application of P $L_{2,3}$-edge XANES to specify P compounds in environmental samples has been restricted by the lack of published reference spectra. To the best of our knowledge the present paper (Table 1, Figs. 2 to 8) provides the most complete overview of P $L_{2,3}$-edge XANES spectra of pure reference compounds and geological P minerals, all measured under consistent experimental conditions. Even though the energy positions of spectral features of some compounds were similar, or differed only marginally, distinguishing them may be possible by intensity differences. Therefore, quantitative analysis by linear combination fitting of P species at the $L_{2,3}$-edge may yield more reliable results than at the *K*-edge. To verify this statement, mixtures with known composition will be measured at the *K*- and $L_{2,3}$-edges and evaluated in conjunction.

Since we observed radiation damage of P-containing organic and inorganic compounds and showed consequences for the P $L_{2,3}$-edge XANES spectra, we conclude that the following measures are required to reduce it. (i) Since the brightness of present day available sources (undulator, wiggler and bending-magnet beamlines) is quite different, the source should be chosen depending on the P concentration in the sample to yield spectra with sufficient signal-to-noise ratios. Tuning the energy transferred to the sample by an appropriate choice of a rather small slit size can further reduce decomposition-related processes. (ii) The exposure time should be reduced by accelerating the scans by a proper choice of the dwell time (*i.e.* integration time per data point). (iii) The beam should be moved to a 'fresh' sample spot after each scan and several scans from different spots should be merged to gain a sufficient signal-to-noise ratio from samples with low P concentration.

The P $L_{2,3}$-edge XANES measurements were performed at the Canadian Light Source (CLS), which is supported by NSERC, NRC, CIHR and the University of Saskatchewan. This work was supported by a travel grant of the German Academic Exchange Service (D/05/50492). The work greatly benefited from the 'Exzellenzförderprogramm' of the Ministerium für Bildung, Wissenschaft und Kultur Mecklenburg-Western Pomerania, project UR 07 079. We thank Dr Heiko Hüneke, Institute of Geography and Geology, University of Greifswald, for providing the minerals used in this study.

References

Ajiboye, B., Akinremi, O. O. & Hu, Y. (2006). *CLS Activity Report 2006.* Canadian Light Source, Saskatoon, Canada.
Ajiboye, B., Akinremi, O. O., Hu, Y. & Jürgensen, A. (2008). *Soil Sci. Soc. Am. J.* **72**, 1256–1262.
Ascone, I., Meyer-Klaucke, W. & Murphy, L. (2003). *J. Synchrotron Rad.* **10**, 16–22.
Beauchemin, S., Hesterberg, D., Chou, J., Beauchemin, M., Simard, R. R. & Sayers, E. (2003). *J. Environ. Qual.* **32**, 1809–1819.
Brandes, J. A., Ingall, E. & Paterson, D. (2007). *Mar. Chem.* **103**, 250–265.
Cade-Menun, B. J. & Preston, C. M. (1996). *Soil Sci.* **161**, 770–785.
Carta, D., Pickup, D. M., Newport, R. J., Knowles, J. C., Smith, M. E. & Drake, K. O. (2005). *Phys. Chem. Glass*, **46**, 365–371.
Domke, M., Mandel, T., Puschmann, A., Xue, C., Shirley, D. A., Kaindl, G., Petersen, H. & Kuske, P. (1992). *Rev. Sci. Instrum.* **63**, 80–89.
Dougherty, W. J., Fleming, N. K., Cox, J. W. & Chittleborough, D. J. (2004). *J. Environ. Qual.* **33**, 1973–1988.
Fendorf, S. E. & Sparks, D. L. (1996). *Methods of Soil Analysis: Chemical Methods*, *SSSA Book Series 5*, edited by D. L. Sparks, pp. 377–416. Madison: Soil Science Society of America.
Franke, R. & Hormes, J. (1995). *Physica B*, **216**, 85–95.
Fuller, M. L. S., Kasrai, M., Bancroft, G. M., Fyfe, K. & Tan, K. H. (1998). *Tribol. Int.* **31**, 627–644.
Godlinski, F., Leinweber, P., Meissner, R. & Seeger, J. (2004). *Nutr. Cycl. Agroecosyst.* **68**, 47–57.
Harp, G. R., Han, Z. L. & Tonner, B. P. (1990). *J. Vac. Sci. Technol. A*, **8**, 2566–2569.
He, Z., Honeycutt, C. W., Zhang, T., Pellechia, P. J. & Caliebe, W. A. (2007). *Soil Sci. Soc. Am. J.* **71**, 940–943.
Hedley, M. J. & Stewart, J. W. B. (1982). *Soil Biol. Biochem.* **14**, 377–385.
Hu, Y. F., Zuin, L., Wright, G., Igarashi, R., McKibben, M., Wilson, T., Chen, S. Y., Johnson, T., Maxwell, D., Yates, B. W., Sham, T. K. & Reininger, R. (2007). *Rev. Sci. Instrum.* **78**, 83–109.
Hunger, S., Sims, J. T. & Sparks, L. (2005). *J. Environ. Qual.* **34**, 382–389.
Kasrai, M., Lennard, W. N., Brunner, R. W., Bancroft, G. M., Bardwell, J. A. & Tan, K. H. (1996). *App. Surf. Sci.* **99**, 303–312.
Kasrai, M., Vasiga, M., Suominen Fuller, M., Bancroft, G. M. & Fyfe, K. (1999). *J. Synchrotron Rad.* **6**, 719–721.
Kasrai, M., Yin, Z. F., Bancroft, G. M. & Tan, K. H. (1993). *J. Vac. Sci. Technol. A*, **11**, 2694–2699.
Khare, N., Hesterberg, D. & Martin, J. D. (2005). *Environ. Sci. Technol.* **39**, 2152–2160.
Kruse, J. & Leinweber, P. (2008). *J. Plant Nutr. Soil Sci.* **171**, 479–658.
Kruse, J., Leinweber, P., Baum, C., Godlinski, F. & Someus, E. (2008). *CLS Activity Report 2007.* Canadian Light Source, Saskatoon, Canada.
Lavrentyev, A. A., Gabrelian, B. V., Dubeiko, V. A., Nikiforov, I. Y. & Rehr, J. J. (2000). *J. Phys. Chem. Solids*, **61**, 2061–2063.
Leinweber, P., Haumaier, L. & Zech, W. (1997). *Biol. Fertil. Soils*, **25**, 89–94.
Li, Y.-R., Bancroft, G. M., Kasrai, M., Fleet, M. E., Feng, X. H. & Tan, K. H. (1994). *Am. Mineral.* **79**, 785–788.
Li, Y.-R., Pereira, G., Kasrai, M. & Norton, P. R. (2008). *Trib. Lett.* **29**, 201–211.
Najman, M. N., Kasrai, M., Bancroft, G. M. & Miller, A. (2002). *Trib. Lett.* **13**, 209–218.
Nordstrom, K. F. & Hotta, S. (2004). *Geoderma*, **121**, 157–167.
Pereira, G., Munoz-Paniagua, D., Lachenwitzer, A., Kasrai, M., Norton, P. R., Capehart, T. W., Perry, T. A. & Cheng, Y.-T. (2007). *Wear*, **262**, 461–470.
Rösler, H. J. (1991). *Lehrbuch der Mineralogie*, 5th ed. Leipzig Dt. Verl. für Grundstoffindustrie.
Schefe, C. R., Kappen, P., Pigram, P. J., Zuin, L. & Christensen, C. (2008). *CLS Activity Report 2007.* Canadian Light Source, Saskatoon, Canada.
Schulze, D. G. & Bertsch, P. M. (1995). *Adv. Agron.* **55**, 1–66.
Shober, A. L., Hesterberg, D. L., Sims, J. T. & Gardner, S. (2006). *J. Environ. Qual.* **35**, 1983–1993.

Sims, J. T., Simard, R. R. & Joern, B. C. (1998). *J. Environ. Qual.* **27**, 277–293.
Siritapetawee, J. & Pattanasiriwisawa, W. (2008). *J. Synchrotron Rad.* **15**, 158–161.
Stöhr, J. (1992). *NEXAFS Spectroscopy*. Berlin: Springer-Verlag.
Toor, G. S., Hunger, S., Peak, J. D., Sims, J. T. & Sparks, D. L. (2006). *Adv. Agron.* **89**, 1–72.
Varlot, K., Kasrai, M., Bancroft, G. M., Yamaguchi, E. S., Ryason, P. R. & Igarashi, J. (2001). *Wear*, **249**, 1029–1035.
Yin, Z., Kasrai, M., Bancroft, G. M., Laycock, K. F. & Tan, K. H. (1993). *Tribol. Int.* **26**, 383–388.
Yin, Z., Kasrai, M., Bancroft, G. M., Tan, K. H. & Feng, X. (1995). *Phys. Rev. B*, **51**, 742–750.
Yin, Z., Kasrai, M., Fuller, M., Bancroft, G. M., Fyfe, K. & Tan, K. H. (1997). *Wear*, **202**, 172–191.
Zubavichus, Y., Zharnikov, M., Shaporenko, A., Fuchs, O., Weinhardt, L., Heske, C., Umbach, E., Denlinger, J. D. & Grunze, M. (2004). *J. Phys. Chem. A*, **108**, 4557–4565.